Structural performance of laser welded edge joints made of high-strength steel

Structural performance of laser welded edge joints made of high-strength steel

Juha Peippo[1], Antti Ahola[2], Timo Björk[2], Antti Salminen[1]

[1]University of Turku, Department of Mechanical and Material Engineering, Finland
[2]Lappeenranta-Lahti University of Technology LUT, LUT School of Energy Systems, Finland

juha.peippo@utu.fi

Abstract. Laser welding is a widely-used fusion welding process in industry. However, laser welding is not a common welding process in the manufacture of industrial crane structures. There has been a remarkable increase in the available strength classes of steel grades over the last 10 years, such that strengths of up to 1200 MPa are now commercially available. This enables the use of thinner materials in welded products and at the same time, has opened up new possibilities for using laser welding more widely in the manufacture of steel structures. This study focuses on the static and fatigue strength of the laser-welded joints. Details investigated are edge joint with flange preparation between two rectangular tubes and edge joint between flat bar and rectangular tube. A novel fatigue strength assessment concept, the FAT_{mod} method, is applied to assess the theoretical fatigue performance of the joint in comparison with the effective notch stress method with a FAT630 design curve. The FAT_{mod} method is based on the local stress ratio at a fatigue-critical point of the joint and the analysis considers the strength of the material, surface quality and applied stress ratio in the assessment of fatigue. The study shows that the samples failed from the base material side in static tests and the FAT_{mod} method developed was found to agree well with the test results.

1. Introduction

Laser welding is a widely-used fusion welding processes in various industrial applications. However, laser welding is not a common welding process in the manufacturing of industrial crane structures. The most frequently-used processes are submerged arc welding (SAW) and gas metal arc welding (GMAW). There has been a remarkable increase in the available strength classes of steel grades over the last decade and strengths of up to 1200 MPa are now commercially available. This has enabled the use of thinner materials in welded structures and consequently, has opened up wider possibilities of utilizing the laser-welding process in the fabrication of steel structures. This has provided not only a change in plate thickness but typically, has stimulated the whole construction process with fresh ideas on how to produce the required performance of the crane. This investigation focuses on the static and fatigue strength of laser welds. The details investigated are edge joint with flange preparation I-type joint between two rectangular tubes and edge joint between flat bar and rectangular tube.

2. Experimental tests

2.1. Test specimens

Two different specimen configurations were used in this study: the first test specimen type consisted of a rectangular hollow section with flat bar and the second consisted of two rectangular hollow sections welded together. The thickness of the flat bars was 25 mm and the steel grade used was normal construction steel S355J2. The rectangular hollow sections were manufactured using a laser-welding process. The material thickness of the rectangular profile was 3 mm and the steel was direct quenched steel S900. Fig. 1 shows the main dimensions of the test samples and the nominal material properties from the literature are shown in Table 1. The conventional carbon equivalent values (CEV) and the other carbon equivalents (PL) for laser weld were calculated [1]. The maximum carbon equivalent values available from steel suppliers are shown in Table 2.

Table 1. Chemical compositions [%] of used steel [1] [2] [3]

	C	Mn	Cr	Mo	V	Cu	Ni	S	Si	P	B
S355J2	0.2	1.6	0	0	0	0	0	0.025	0.55	0.025	0
Optim900QC	0.20	1.6	0.8	0.7	0	0.3	2	0.01	0.05	0.03	0

Table 2. Mechanical properties of used steel. [3] [4]

	f_y [MPa]	f_u [MPa]	A_5 [MPa]	CEV/CEVmax	LP
S355J2	355	460	23	0.47/0.45	0.27
Optim 900 QC	900	950	7	0.92/0.58	0.27

The test pieces were 100 mm long and were cut from longer sections, about 1000 mm long see Fig. 1. All welds were produced without filler material.

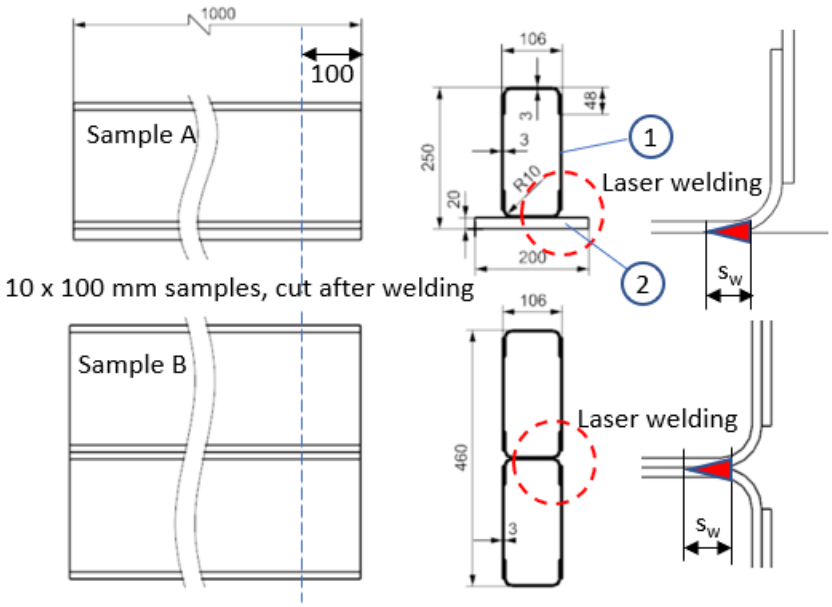

Fig. 1. The shape and main dimensions of the test samples. a) laser weld joint between S355J2 rectangular profile and HS-steel profile and b) laser weld joint between two HS-steel hollow-profile. (red arrows show laser-weld seam positions; thickness of part 1 is 3 mm and part 2 is 20 mm; width of part 2 is 200 mm)

The welding processes was carried out using a CO2-laser welding machine. The welding power was 4.4 kW and welding speed was ether 1.50 m/min or 2.50 m/min. The average width of the weld was about 0.9 mm and penetration s_w was about 4.7 mm in edge joint seams; see Fig. 1 . The laser machine type used was a CO2-Laser Rofin Sinar 4.5 kW and the shielding gas used was helium. Gas flow was 10 l/min. All weldings were performed at normal room temperature of about 20 °C without preheating the welding. The welding parameters are seen in Table 3. Focus = 0 means the laser beam was adjusted so that its focal point was on the surface of test specimen.

Table 3. Used welding parameters and approximation of heat input values Q.

Joint	Focus [mm]	Power [kW]	Speed [mm/min]	Gas	Q [kJ/mm]
Plate and O-profile		4.4	2500	Helium/10 l/min	0.07
Two O-profiles joint	0	4.4	2500	Helium/10 l/min	0.07
Lap joint		4.4	1500	Helium/10l/min	0.12

Heat input values Q were calculated based on Eq.(1) that is given in standard SFS-EN 1011-1

$$Q = k \cdot \frac{P}{v \cdot 1000} \quad (1)$$

where k is thermal coefficient, P is power [W] and v is welding speed [mm/s]. The Eq. (1) gives results in unit kJ/mm. The thermal coefficient, which SSAB proposed to use for laser weld [5], was selected 0.7.

2.2. Static tensile tests

In order to validate the ultimate performance of the structure, static tests were carried out. The tensile test setup is presented in Fig. 2. The samples were clamped to the table of the test ring and external force was applied to the test pieces through the rigid yoke.

Sample A Sample B Potential failure locations

Fig. 2. Test setups for samples A and B. The red arrows show cylinder force directions in the test ring. Potential failure locations.

There were six tensile tests in total. The tensile strength results and typical failure modes are shown in Fig. 3. The average depth s_w of the laser-weld seams was about 4 mm. The ultimate load carrying capacity was 139 kN for sample A and 114 kN for sample B, respectively. The rupture location was at the weld toe outer side of the beam and the fracture passed perpendicularly through the wall thickness of the base material. The nominal tensile capacity of the webs of the hollow profile is 540 kN (f_y·area). This means that the capacity of the formed and welded area related to the capacity of the webs is 0.26 for sample A and 0.21 for sample B.

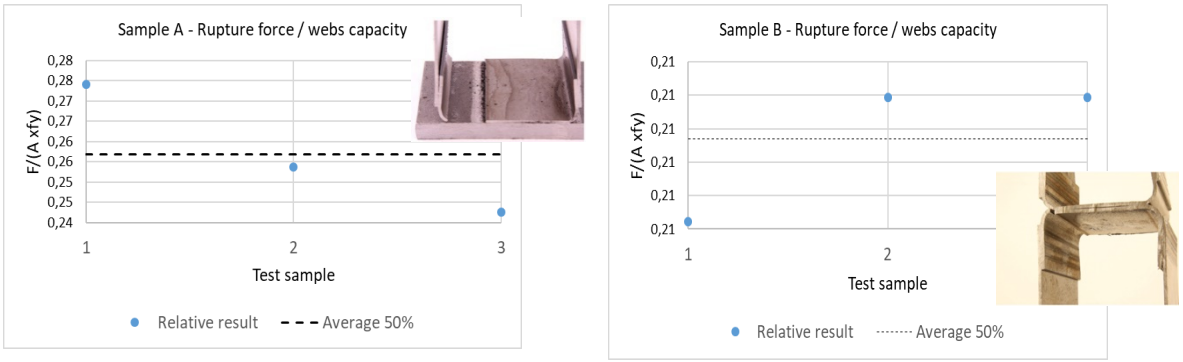

Fig. 3. The tensile strength test results for samples A and B.

2.3. Fatigue tests

Fatigue tests were carried out in the steel structures laboratory at LUT University. The tests were performed using constant amplitude loading, and the stress ratio R was set at close to 0.1, as shown in Table 4. The test matrix and test results are presented in Table 4. The nominal membrane stress range in the webs, equal to F / A_w, is presented in Table 4. The reference area used is $A_w = 600$ mm^2.

The locations of the fatigue failures are shown in Fig. 2. Point 1 illustrates the crack through the base material, Point 2 the crack at the weld toe propagating in the base material and Point 3 the crack at weld root propagating in the base material, respectively.

Table 4. Test matrix and the results of fatigue tests.

Sample	F_{max} / F_{min} [kN]	R [-]	Δσ at web [MPa]	N_f [cycles]	Failure
A-KO_4	10.40 / 0.20	0.02	17.1	102000	Point 1, at end of profile
A-KO_5	35.66 / 0.20	0.01	59.1	1438	Point 1, at end of profile
A-KO_6	9.93 / 0.20	0.02	16.2	25440	Point 1, at end of profile
A-KO_7	15.30/5.00	0.33	17.2	63452	Point 1, at end of profile
A-KO_8	12.06 / 0.00	0.00	20.1	13920	Point 1, at end of profile
A-KO_9	12.35 / 0.31	0.03	20.1	13560	Point 1, at end of profile
A-KO_12	93.13 / 0.85	0.01	153.8	180	Point 1, at end of profile
B-KOA1_1	10.34 / 0.17	0.02	16.9	139962	Point 1, at end of profile
B-KOA1_2	10.28 / 0.24	0.02	16.7	129686	Point 1, at end of profile
B-KOA1_3	10.34 / 0.28	0.03	16.8	122854	Point 1, at end of profile
B-KOA1_4	12.36 / 0.25	0.02	20.2	36478	Point 1, at end of profile
B-KOA1_5	12.35 / 0.24	0.02	20.2	34730	Point 1, at end of profile
B-KOA1_6	12.50 / 0.39	0.03	20.2	91500	Point 1, at end of profile
B-KOA1_7	12.17 / 0.20	0.02	19.9	71492	Point 1, at end of profile

The depth of the weld seams was measured after the failure for four test samples. The selected samples were assumed to present a typical cross section of weld seam shapes, and two joints were investigated in detail, as illustrated in Figure 7. The measured mean penetration s_w was 4 mm for sample A and 4.55 mm for sample B. These values were subsequently used in this investigation and are slightly different than the values obtained from the test samples used in the static tests.

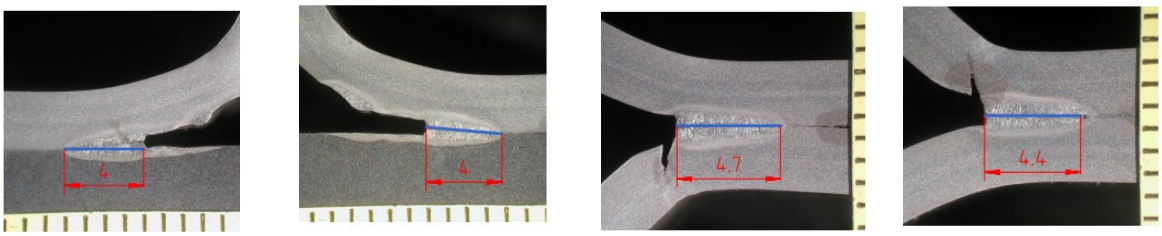

Sample A Sample B

Fig. 4. Typical depth of weld seams.

3. FE-models

The linear-elastic stress concentration factors K_t are needed in fatigue strength assessment of the joints using the notch stress concepts. These were determined with the FE method at both the weld toe and weld root sides of the laser weld in the flange groove. Parabolic tetra elements were used. The effective notch stress approach was applied and a fictitious notch radius of r = 0.05 mm was applied in the model in accordance with the recommendations for a thin-walled joint (t < 5mm) [6]. Six elements over the 45-degree arc were used in the models, fulfilling the mesh density requirement proposed by Fricke [7] .

Double symmetry was exploited and a linear material model was used. Young's modulus E = 210000 MPa and Poisson ratio ν = 0.3 were used. The gap between connected palates was assumed to be zero, and no contact configuration was applied to this gap.

The external tensile force was applied to the models through a yoke and the value of the force was 3750 N in one quarter FE model. The yoke was connected to the rectangular hollow section using a contact boundary condition. The friction value was set to be 0.2 in this contact area. The measured average values for weld dimensions were used in FEA. Fig. 5 presents the mesh and boundary conditions used in FEA.

The stress concentration factors were calculated in three different locations. The factors $K_{t,w,t}$ and $K_{t,w,r}$ were calculated based on stress distribution through the weld seam, while the stress concentration factor $K_{t,b,t}$ was determined based on stress distribution through the plate thickness at the boundary line between the weld and the base plate, corresponding to the potential fatigue failure paths in the studied laser welds. The calculated stress distributions $\sigma(x)$ were divided in membrane-, bending- and non-linear stress components, as shown in Fig. 5. Separation was carried out by applying the widely-used Eqs presented in reference [8].

Linear-elastic notch stress concentration factors were calculated using the following formula

$$K_t = \frac{\sigma_{memb} + \sigma_{bend} + \sigma_{nlp}}{\sigma_{memb} + \sigma_{bend}} \quad (2)$$

The stress components and absolute stress concentration factors are given in Table 5. Stresses were calculated with external force 3750 N in test setup.

Table 5. Selected stresses and the stress concentration values. K_t . Membran stress component is compress, because the yoke does not be rigid and external force effects on the middle of the yoke.

	σ_{memb}	σ_{bend}	σ_{nlp}	$\lvert K_t \rvert$	Stress path (see Fig. 8)
$K_{t,w,t}$	-69	143	1112	16.0	sample A, Line 1
$K_{t,w,r}$	-69	-143	1002	3.7	sample A, Line 1
$K_{t,b,t}$	-14	515	1775	4.5	sample A, Line 2
$K_{t,w,t}$	-120	42	1161	13.9	sample B, Line 1
$K_{t,w,r}$	-120	-42	-552	4.4	sample B, Line 1
$K_{t,b,t}$	-28	491	1159	3.5	sample B, Line 2

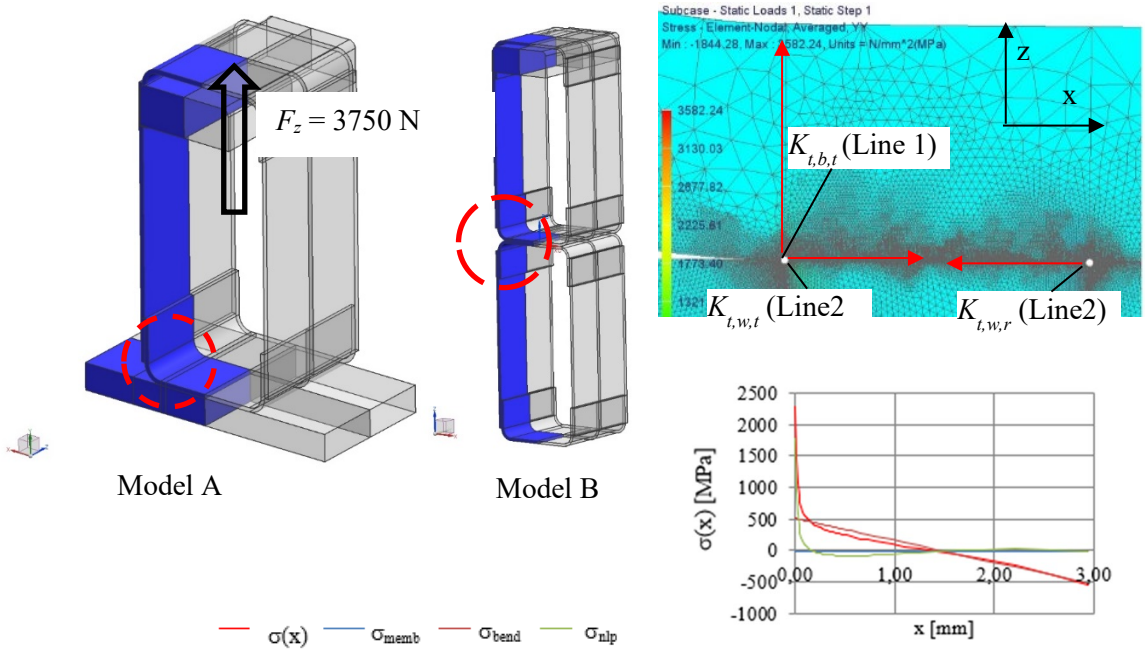

Fig. 5. The type of test samples and detail of mesh in FE models that were used in the determination of stress concentration factors. Lines 1 and 2 show the stress plotting lines that were used in subsequent calculations. The stresses were read in nodes on the outer surface part. Example stress distribution from line 1 and stress components (x is distance from critical point).

4. Fatigue strength assessment of the joints

4.1. Modified notch stress approach

The fatigue strength of laser-welded joints is evaluated by means of a modified local stress approach, with reference to Nykänen et al. [9] [10] [11], Björk et al. [12] and Peippo et al. [13].

The linear-elastic stresses and strains were transformed to elastic-plastic (σ_1, ε_1) components by using Eq. (5)

$$\left.\begin{aligned} \varepsilon_1 \cdot \sigma_1 &= \frac{\left(K_{fmod} \cdot \sigma_{nom,max} + \sigma_r\right)^2}{E} \\ \varepsilon_1 &= \frac{\sigma_1}{E} + \left(\frac{\sigma_1}{K'}\right)^{1/n'} \end{aligned}\right\} \rightarrow output\ \sigma_1\ and\ \varepsilon_1 \tag{3}$$

where $\sigma_{nom,max}$ is the maximum nominal stress, σ_r is residual stress, E is Young's modulus, n' is the cyclic strain hardening exponent, and K' is the cyclic strength coefficient. In this investigation n′ is 0.164 and $K' = 1.65 \cdot f_u$ [14]. K_{fmod} is a notch-sensitive factor, that is calculated according to Eq. (6). The effect on surface quality is taken into account in Eq. (6) through the term $C_{\sigma R}$, that is, the roughness correction factor for axial stress. Factor $C_{\sigma R}$ is calculated using Eq. (7).

$$K_{fmod} = \left(K_f + \frac{1}{C_{\sigma R}} - 1\right) \tag{4}$$

$$C_{\sigma,R} = 1 - a_R \cdot log(R_z) \cdot log\left(\frac{2 \cdot f_u}{S_{u,min}}\right) \tag{5}$$

where a_R is a roughness constant (for steel a_R is 0.22), $S_{u,min}$ is minimum ultimate tensile strength (for all structural steel $S_{u,min}$ is 400 MPa [15]), R_z is the roughness value of the surface in [µm] and f_u is the ultimate strength of the material.

Elastic-plastic stress and strain ranges are calculated ($\Delta\sigma$, $\Delta\varepsilon$) by using Eq. (8). This equation is based on Neuber's rule and kinematic hardening rules

$$\left.\begin{aligned} \Delta\varepsilon \cdot \Delta\sigma &= \frac{\left(K_{fmod} \cdot \Delta\sigma_{nom}\right)^2}{E} \\ \Delta\varepsilon &= \frac{\Delta\sigma}{E} + 2\left(\frac{\Delta\sigma}{2 \cdot K'}\right)^{1/n'} \end{aligned}\right\} \rightarrow output\ \Delta\sigma\ and\ \Delta\varepsilon \quad (6)$$

where $\Delta\sigma_{nom}$ is nominal stress range in the location under investigation. True stress ration R_{true} is calculated by the equation (9). The stress ratio R_{true} values were limited between -2 to 0.5.

$$\left.\begin{aligned} \sigma_2 &= \sigma_1 - \Delta\sigma \\ R_{true} &= \frac{min(\sigma_1, \sigma_2)}{max(\sigma_1, \sigma_2)} \end{aligned}\right\} \rightarrow output\ \sigma_2\ and\ \ R_{true} \quad (7)$$

All stresses are commeasured into a reference stress system, corresponding to the true stress ratio of $R_{true} = 0$. A Smith-Watson-Topper (SWT) mean stress correction is applied to define a new stress range $\Delta\sigma_{ref,R=0}$ referring the equivalent stress range, when $R = 0$, according to Eq. (10)

$$\Delta\sigma_{ref,R=0} = \frac{K_{fmod} \cdot \Delta\sigma_{nom}}{\sqrt{1 - R_{true}}} \quad (8)$$

4.2. Stress ranges

The fatigue test results are tabulated in Table 6 and the stress ranges calculated using the linear stress concentration factor are given in Table 5. Thus, the linear stress calculation equations can be carried out according to Eqs. (9) – (11).

$$\Delta\sigma_1 = K_{t,b,t} \cdot \Delta\sigma_{nom} \quad (9)$$

$$\Delta\sigma_2 = K_{t,w,t} \cdot \Delta\sigma_{nom} \quad (10)$$

$$\Delta\sigma_3 = K_{t,w,r} \cdot \Delta\sigma_{nom} \quad (11)$$

The stress range is calculated using Eq. (12). The calculated stress range can be positive or negative depending on the stress component values.

$$\Delta\sigma_{nom} = \sigma_1 - \sigma_2 \quad (12)$$

Table 6. Fatigue test results and stress ranges based on linear stress calculation and linear stress concentration factors

Test sample	Point 1 $\Delta\sigma_1$ [MPa]	Point 2 $\Delta\sigma_2$ [MPa]	Point 3 $\Delta\sigma_3$ [MPa]	N_f [cycles]	Failure location	Test sample	Point 1 $\Delta\sigma_1$ [MPa]	Point 2 $\Delta\sigma_2$ [MPa]	Point 3 $\Delta\sigma_3$ [MPa]	N_f [cycles]	Failure location
A-KO_4	1553	811	-829	102000	Point 1	B-KOA1_1	1099	-733	-484	139962	Point 1
A-KO_5	5374	2804	-2869	1438	Point 1	B-KOA1_2	1085	-724	-478	129686	Point 1
A-KO_6	1475	770	-788	25440	Point 1	B-KOA1_3	1087	-725	-479	122854	Point 1
A-KO_7	1562	815	-834	63452	Point 1	B-KOA1_4	1309	-874	-577	36478	Point 1
A-KO_8	1826	953	-975	13920	Point 1	B-KOA1_5	1308	-874	-577	34730	Point 1
A-KO_9	1826	953	-975	13560	Point 1	B-KOA1_6	1308	-874	-577	91500	Point 1
A-KO_12	13992	7302	-7470	180	Point 1	B-KOA1_7	1293	-863	-570	71492	Point 1

4.3. **Modified fatigue strength FAT_{mod} using the reference stress ratio**

The mean FAT_m classes were calculated for Point 1, where the fatigue failures occurred. The reference stress component $\Delta\sigma_{ref,R=0}$ is used in regression analyses. The slope of the S-N curve is set to be $m = 3$. For comparison, the regression analyses were also conducted by using free slope S-N curves. The calculated mean reference $FAT_{m,Rtrue=0}$ and characteristic $FAT_{c,Rtrue=0}$ values are given in Table 7 and the S-N curves are plotted in Fig. 7. In the calculations it was assumed that no residual stresses exist and that surface quality $R_z = 100$ (the surface quality was only an estimate).

The effect on the residual stress assumption to deviation value in regression analyses is estimated in Fig. 11. The value of the residual stress was varied in relation to material yield strength, initial residual stress values were calculated with Eq. (13), and the results were applied in Eq. (5).

$$\sigma_r = f \cdot f_y, \tag{13}$$

where f is scaling factor that vary from -1 to 1 with interval 0.2.

The minimum deviation was given with the residual stress assumption that f is -0.4, as shown in Fig. 6. The regression analyses were repeated using that initial residual stress assumption. The results are given in Table 7 and in Fig. 7.

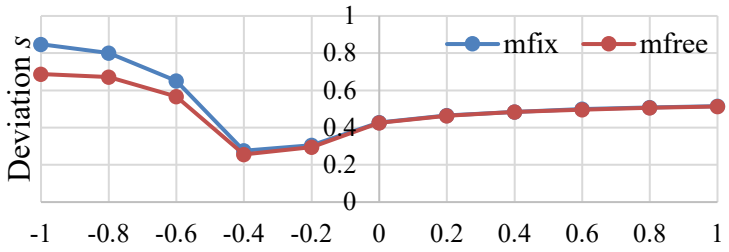

Fig. 6. Deviation vs. residual stress assumption in regression analyses.

Table 7. Reference FAT-classes and deviations.

Test sample	Residual stress	Location	m_{fixed}	$FAT_{m,Rtrue=0}$ and deviation	$FAT_{c,Rtrue=0}$	m_{free}	$FAT_{m,Rtrue=0}$ and deviation	$FAT_{c,Rtrue=0}$
A+B	0	Line 1	3	137 0.427	53	2.9	131 0.426	49.0
A+B	-0.4· f_y	Line 1	3	107.7 0.276	58	2.5	83.2 0.236	44.8

The comparison between fatigue test results and calculated fatigue life estimations were given in Fig. 8. The residual stress assumption was varied between 0 (A) and -0.4f_y (B). Residual stresses were calculated by using the smallest yield strength of the detail. Dotted lines were plotted by using 95% confidential level.

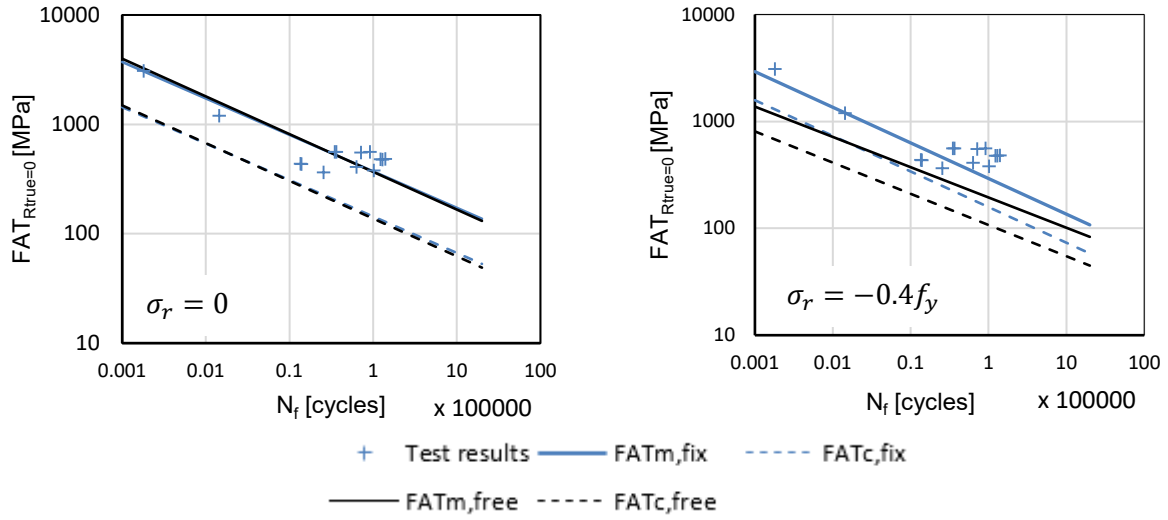

Fig. 7. S-N-curve based assumption of non-existing residual stresses and residual stress assumption -0.4· f_y, and surface roughness of R_z =100.

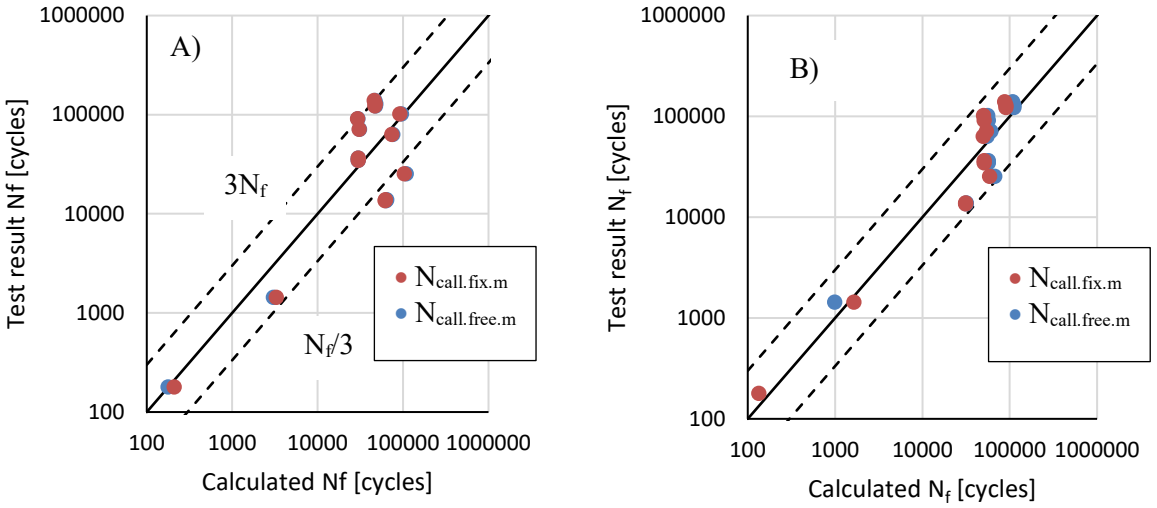

Fig. 8. Tested fatigue time vs. calculated fatigue time with a 95% confidence level (dotted lines) and with residual stress assumption σ_r = 0 MPa in figure A and σ_r = -0.4f_y MPa in figure B

4.4. Comparison of the modified fatigue strength FAT_{mod} and effective notch stress methods

The effective notch stress method gives a constant FAT class of 630 MPa, when the effective notch radius is 0.05 mm [7]. Linear notch stress is used and the slope of the SN-curve is m = 3. Fatigue life predictions generated using ENS and FAT_{mod} methods are presented in comparison with the test results in Fig. 9. Calculated lives were obtained with the characteristic values. Results show that the ENS results are unconservative (below the black line of the constant) while FAT_{mod} results are conservative (located above the black line). Furthermore, it is worth mentioning that the FAT_{mod} method is able to predict, for example, the effect of different parameters, such as applied stress ratio, see Eq. (5), on fatigue strength, and thus enabling more accurate estimations of fatigue life.

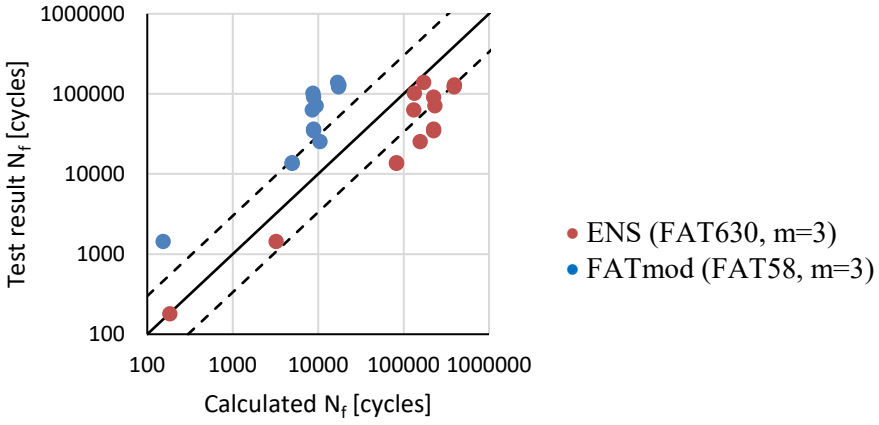

Fig. 9. Calculated fatigue time estimations.

5. Conclusion

In this research work static and fatigue experimental tests for laser-welded joints made of normal and ultra high strength structural steels were carried out. The results were compared with numerical values

obtained through a modified local strain approach. Based on these results the following conclusions can be drawn:

- Nominal static performance of joint compared to capacity of wall thickness in pure tension is rather low, equal to 0.21–0.26 of the web capacity.
- The results indicate that the FAT_{mod} method has the capability to describe stress states and it gives a reasonably accurate fatigue time estimation for the details that were investigated. However, the number of test samples was limited and to obtain greater reliability, further tests are needed.
- The fatigue life comparisons indicated that the ENS method with FAT630 (r = 0.05 mm) gives an unconservative fatigue life estimation in comparison with the investigated FAT_{mod} method for the laser welds studied.
- Deviation in the statistical analyses was lowest when the residual stress assumption in the equations was equal to $\sigma_r = -0.4 f_y$.

6. Acknowledgments

This work was funded by the Research Fund. The Research Council is further acknowledged for support.

ORCID IDs

A Ahokas https://orcid.org/0000-0001-8706-5680
A Salminen https://orcid.org/0000-0002-9071-3682
J Peippo https://orcid.org/0000-0001-5681-3877
T Björk https://orcid.org/0000-0001-8870-5678

7. List of references

[1] "B2B Metel. Online metalll marketplace," [Online]. Available: http://www.b2bmetal.eu/en/pages/index/index/id/149/. [Accessed 23 10 2016].

[2] “Steel Express,” [Online]. Available: http://www.steelexpress.co.uk/structuralsteel/S355-S275-structural-steel.html. [Accessed 23 10 2016].

[3] “Strength 900 datat sheet,” SSAB, [Online]. Available: http://www.ssab.fi/tuotteet/brandit/strenx/tuotteet/strenx-900. [Accessed 23 10 2016].

[4] “Grand steel,” [Online]. Available: http://gangsteel.net/product/alloy/en100252//s355j2.html. [Accessed 23 10 2016].

[5] SSAB, “WeldCalc 2.2 calculation program,” SSAB, 2012.

[6] C. Sonsino, W. Fricke, F. Bruyne, A. Ahmadi and G. Zhang, Notch stress concepts for the fatigue assessment of welded joints - Background and applications, International Journal of Fatigue, 34 (2012) 2-16.

[7] W. Fricke, “IIW-Doc. XIII-2240r2-08/XV-1289r2-08 IIW Recommendations for the Fatigue Assessment by Notch Stress Analysis for Welded Structures,” 2010.

[8] A. Hobbacher, “IIW document XIII-1965-03 / XV-1127-03 Recommendations for fatique design of welded joints and components”.

[9] T. Nykänen and T. Björk, “A new proposal for the assessment of fatigue strength of steel butt-welded joints improved by peening. IIW International Conference. High-Strength Materials – Challenges and Applications, 2-3 July 2015, Helsinki, Finland”.

[10] T. Nykänen and T. Björk, “A new proposal for assessment of the fatigue strength of steel buttwelded joints improved by peening (HFMI) under constant amplitude tensile loading,” in *FFEMS Fatigue & Fracture of Engineering Materilas & Structures* , 2016, pp. 566-582.

[11] T. Nykänen and T. Björk, “Assessment of fatigue strength of steel buttwelded joints in as-welded condition - Alternative approaches for curve fitting and mean stress effect analysis,” in *Marine Structures 44*, 2015, pp. 288-310.

[12] T. Björk, H. Mettänen, A. Ahola and M. Lindgren, “Fatigue strerength assessment of duplex and super-duplex stainless steel by 4R method,” in *IIW : XIII-2683-17*, 2017.

[13] J. Peippo, T. Björk and T. Nykänen, “A novel method for fatigue assessment of steel plates with thermally, Welding in the World (2018) 62:105-115, https://link.springer.com/article/10.1007/s40194-017-0529-7,” 2017.

[14] D. Radaj, C. Sonsino and W. Fricke, “Fatigue assessment of welded joint by local approaches. 2nd edition. Cambridge: Woodhead Publishing,” 2006.

[15] B. Hänel, E. Haibach, T. Seeger, G. Wirthgen and H. Zenner, “FKM-Guidline. Analytical strength assessment. 5th Edition. ISBN 3-8163-0425-7,” 2003.

[16] “Ruukin kuumavalssatut erikoisteräkset,” Ruukki Oy, 16 5 2012. [Online]. Available: https://wiki.oulu.fi/.../Ruukin+kuumavalssatut+erikoisteräkset+-+Olli+Vähäkainu.pdf. [Accessed 9 10 2016].

[17] J. Peippo, A modified nominal stress method for fatigue assessment of steel plates with thermally cut edges, Lappeenranta: Acta Universitatis, 2015.

[18] M. Ysuyama, H. Gujimoto, M. Uchihara and K. Fukui, IIW: III-1380-06. The Laser welded joint stregth of advanced automotive high strength steel sheets.